Sensors and Materials, Vol. 35, No. 12 (2023) 4203–4214
MYU Tokyo

S & M 3476

Conductive Diamond-like Carbon Microneedle Electrode for Electrochemical Sensors

Takeshi Kondo,[1,2*] Azusa Sato,[1] Masanori Hiratsuka,[3] and Makoto Yuasa[1,2]

[1]Department of Pure and Applied Chemistry, Faculty of Science and Technology, Tokyo University of Science, 2641 Yamazaki, Noda 278-8510, Japan
[2]Research Institute for Science and Technology, Tokyo University of Science, 2641 Yamazaki, Noda 278-8510, Japan
[3]Nanotec Corp., Nanotechno-Plaza, 4-6 Kashiwa-Inter-minami, Kashiwa, 277-0874, Japan

(Received September 11, 2023; accepted October 13, 2023)

Keywords: diamond-like carbon (DLC), microneedle electrode, electrochemical detection, electrode fouling

A conductive diamond-like carbon (DLC) electrode was prepared by coating a conductive DLC thin film onto a silicon substrate surface using high-power impulse magnetron sputtering (HiPIMS) and ionization deposition methods. The resulting DLC electrode showed a wide potential window of ~3 V. Its background current was slightly larger than that of the boron-doped diamond (BDD) electrode and much smaller than that of the glassy carbon electrode, indicating that the DLC electrode has electrochemical properties similar to those of the BDD electrode. Electrochemical measurements in phosphate buffer solution (PBS) containing bovine serum albumin (BSA) did not result in electrode fouling, suggesting that the DLC electrode is suitable for highly sensitive electrochemical measurements in biological fluids. Furthermore, conductive DLC was deposited on the tip of a glass needle to fabricate a DLC microneedle (DLC-MN) electrode with a small tip diameter of 600 nm. The DLC-MN electrode exhibited typical microelectrode behavior and was used to determine ascorbic acid and theophylline in PBS containing BSA. With its small tip diameter and excellent fouling resistance, the DLC-MN electrode holds great promise for facilitating highly sensitive and stable local electrochemical sensing or monitoring *in vivo*.

1. Introduction

Microneedle electrodes can be used in electrochemical devices to detect and monitor electroactive compounds in the local spaces of living organisms.[1–3] For example, microneedle or microneedle electrode arrays have been employed for minimally invasive electrochemical detection or monitoring of various substances, including glucose,[4,5] lactate,[6] alcohol,[7] and levodopa,[8] within dermal interstitial fluids. Furthermore, rod-shaped electrodes with microneedles at their tips[9] have been used for deep tissue insertion in animals to detect biological substances and drugs in the body.[10] Metals[4,5,7,9] and carbons[11] have been used as

*Corresponding author: e-mail: t-kondo@rs.tus.ac.jp
https://doi.org/10.18494/SAM4656

ISSN 0914-4935
https://myukk.org/

materials for microneedle electrodes, but boron-doped diamond (BDD) can perform stable electrochemical detection owing to its excellent resistance to electrode fouling caused by protein adsorption to the electrode surface.[12,13] Ogata *et al*. reported that a drug-sensing system comprising a glass microelectrode and a BDD microneedle electrode enabled simultaneous sensing of the bumetanide concentration and endocochlear potential in guinea pig cochlea.[14] Basically, reducing the tip diameter of a microneedle electrode can create a less invasive device ideal for electrochemical detection in microenvironments. However, there is a limitation inherent to BDD—its crystalline nature constrains the reduction of microneedle tip diameters beyond the BDD crystallite size.

Diamond-like carbon (DLC) is an amorphous material that can be formed into nanometer-thick thin films with dense, homogeneous, and smooth surfaces on various substrate materials via low-temperature processes. DLC has superior biocompatibility and finds applications in medical device coatings and cell culture.[15] Generally, DLC exhibits low electrical conductivity, but its electrical properties can be tailored through doping and composition control, particularly its sp^2/sp^3 carbon ratio.[16,17] This renders the conductive DLC thin film suitable for electrochemical electrodes, as evidenced by their successful applications in detecting substances such as glucose.[18,19] Therefore, conductive DLC is suitable for microneedle electrodes with small tip diameters. Herein, we fabricated a conductive DLC microneedle (DLC-MN) electrode with a glass needle substrate and evaluated its electrochemical properties. We primarily investigated the fouling resistance of DLC-MN electrodes in protein-containing electrolytes in consideration of applications as electrochemical sensors used in biological fluid matrices.

2. Experimental Methods

The conductive DLC thin films were produced by Nanotec Co., Ltd. by the high-power impulse magnetron sputtering (HiPIMS) method[20] and the ionization deposition method on conductive silicon wafer substrates. In the HiPMS method, a DLC thin film was coated on the substrate surface under argon gas at a substrate voltage of 900 V and a target voltage of 1000 V for 15 min. The ionization deposition method involved the deposition of a boron-doped DLC thin film on the substrate surface using 3.5 sccm of acetylene and 0.3 sccm of trimethylborate. The process parameters included a substrate voltage of 2 kV, an anode voltage of 60 V, a filament current of 30 A, and a deposition time of 3 min. Subsequently, the DLC thin film underwent UV/ozone treatment using a UV/ozone processor (SSP17-110, Sen lights Corp.) for 30 min.

Conductive DLC-coated microneedles were fabricated by depositing a DLC layer onto glass microneedles, which were prepared by pulling a borosilicate glass rod (BR-100-10, Sutter) using a micropipette puller (P-2000, Sutter). To enhance adhesion and conductivity between the glass and the DLC film, a titanium layer was coated on the glass needles using RF magnetron sputtering. Subsequently, a conductive DLC thin film was coated onto these microneedles by the HiPMS and ionization deposition methods to obtain conductive DLC-MNs.

The prepared conductive DLC thin film and conductive DLC-MN were characterized by Raman spectroscopy (NRS-5100, Jasco), laser microscopy for DLC thin films (VK-X200, Keyence), scanning electron microscopy for DLC-MN (SEM, JSM-7600F, Jasco), and X-ray photoelectron spectroscopy (XPS, Axis-Nova, Kratos).

Electrochemical measurements were performed using a potentiostat (HZ-7000, Hokuto Denko) with a platinum wire as the counter electrode and an Ag/AgCl electrode as the reference electrode. For electrode fouling experiments, bovine serum albumin (BSA, Fujifilm Wako) was used as a model protein. Comparative electrochemical experiments were performed using a BDD thin-film electrode, a glassy carbon (GC, BAS, 3 mm in diameter) electrode, and a platinum microelectrode (BAS, 10 μm in diameter), with the BDD electrode prepared in our laboratory as described in previous reports.[21]

3. Results and Discussion

3.1 Electrochemical properties of conductive DLC thin films

Figure 1 shows the Raman spectra of DLC thin films deposited on silicon substrates by the HiPMS and ionization deposition methods. The peak in the Raman shift range of 1150–1750 cm^{-1} could be deconvoluted into two bands: the D band (~1350 cm^{-1}) and the G band (~1550 cm^{-1}). The ratios of peak intensities between the D and G bands (I_D/I_G) were 0.58 and 0.65 for the thin films prepared by the HiPMS and ionization deposition methods, respectively. Amorphous carbon films, including DLC, can exhibit diverse properties depending on the deposition method and conditions. They are often classified in accordance with the composition ratios of sp^2 carbon, sp^3 carbon, and hydrogen.[17] In general, DLC thin films with a large amount of sp^2 carbon, indicating a substantial amount of conductive graphitic component, tend to show high G band intensities. Conversely, as the proportion of sp^3 carbon increases, the G band intensity decreases, and the D band intensity increases relative to the G band intensity. Within this broad spectrum of amorphous carbon film compositions, the sp^2/sp^3 carbon composition ratios of the DLC thin films prepared by the HiPMS method and the ionization deposition method in this study were remarkably similar. The HiPMS method, using a carbon target, forms films only with carbon, whereas the ionization deposition method, employing acetylene/trimethyl borate as the carbon source, yields DLC thin films containing hydrogen and boron. Despite such a difference in composition, no noticeable difference in electrochemical

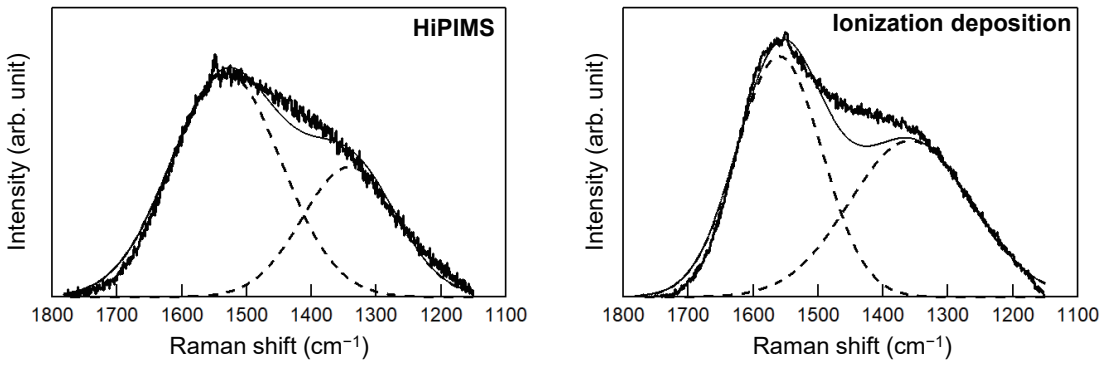

Fig. 1. Raman spectra of DLC thin films prepared by (a) HiPIMS and (b) ionization deposition methods. Thick solid line: experimental curve, dashed lines: D (~1350 cm^{-1}) and G (~1550 cm^{-1}) bands, and thin solid line: simulated curve.

properties was observed, as will be described later. The conductivity of DLC is mainly attributed to the graphitic components contained in the thin film.[22] Consequently, the similar sp^2/sp^3 carbon composition ratios of the thin films deposited by the two deposition methods suggest that those thin films exhibited analogous electrochemical properties, highlighting the comparable nature of their conductivity and performance.

The surface roughness of the DLC thin film was examined through laser microscopy (not shown), revealing that both the DLC thin films prepared by the HiPMS and ionization deposition methods exhibited uniform and flat surfaces. The average surface roughness (S_a) of these thin films was 9 nm. In contrast, the BDD electrode comprised a polycrystalline BDD thin film, manifesting a rougher surface than DLC owing to its submicrometer-sized crystal grains, with S_a of 354 nm. In addition, to cover the entire substrate with a BDD thin film, a film thickness equivalent to the BDD crystal grain size is required (typically 1 μm or more). Conversely, DLC, an amorphous material, boasts a surface with nanometer-sized smoothness and can cover the entire substrate with a thin-film thickness of ~75 nm. This trait not only facilitates the fabrication of electrodes with smooth surfaces but also allows for producing DLC electrodes on microstructured substrates. This observation suggests that DLC is more suitable than BDD for fabricating microneedle electrodes with small tip diameters by coating.

Figure 2(a) shows the cyclic voltammetry (CV) profiles for the GC, BDD, and DLC electrodes in 0.1 M Na_2SO_4. Notably, the potential window of the DLC electrodes was >3 V, wider than that of the GC electrode and comparable to that of the BDD electrode. Furthermore, the background current of the DLC electrode was much lower than that of the GC electrode but higher than that of the BDD electrode. This result indicates that the electrochemical properties of the DLC electrode, comprising sp^3 and sp^2 carbons, fall between those of the GC electrode (dominated by sp^2 carbon) and the BDD electrode (predominantly sp^3 carbon). Importantly, the wide potential window and low background current of the DLC electrode are properties close to those of the BDD electrode. Figure 2(b) shows the CV profiles of 1 mM $Ru(NH_3)_6Cl_3$ in 0.1 M $HClO_4$ for the

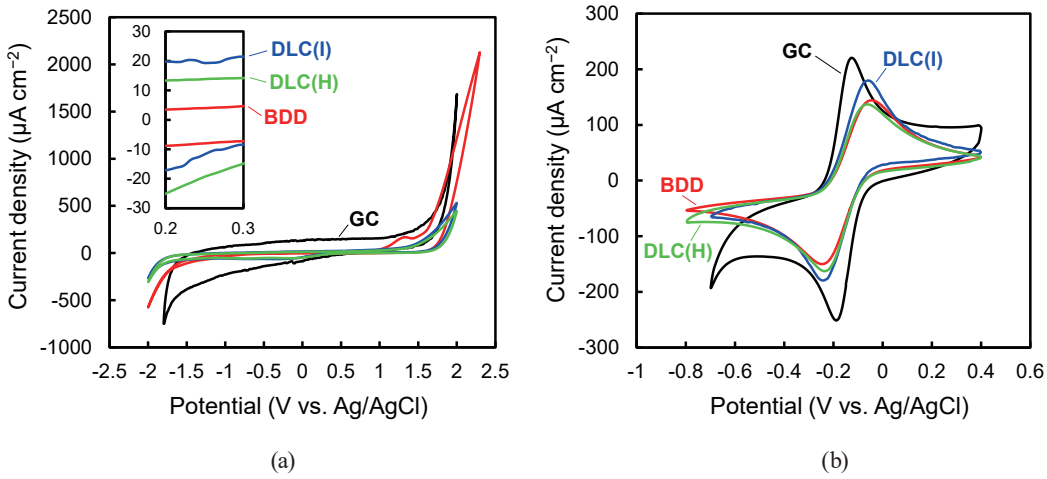

Fig. 2. (Color online) CVs (a) in 0.1 M Na_2SO_4 and (b) for 1 mM $Ru(NH_3)_6Cl_3$ in 0.1 M $HClO_4$ at GC, BDD, DLC(H) (HiPIMS), and DLC(I) (ionization deposition) electrodes. The potential sweep rate was 100 mV s^{-1}. Inset of panel (a) indicates a magnification of the curves.

GC, BDD, and DLC electrodes. These electrodes showed typical reversible/quasi-reversible CV behavior. The CV profile of $Ru(NH_3)_6^{2+/3+}$ is less affected by the functional groups on the electrode surface but affected by the conductivity of the electrode.[23] Thus, an anodic–cathodic peak separation of ~180 mV for both the BDD and DLC electrodes suggests that the DLC electrode is as conductive as the BDD electrode, whereas it was 60 mV for the CG electrode. Furthermore, the results of the CV for $Ru(NH_3)_6^{2+/3+}$ indicated that the DLC electrode had electrochemical properties closer to those of the BDD electrode than to those of the GC electrode. Given its wide potential window and considerably low background current, the DLC electrode is poised to offer a large signal-to-background ratio, making it suitable for application in highly sensitive electrochemical detection.

We investigated the CV of 1 mM ascorbic acid (AA) in 1/15 M phosphate buffer solution (PBS, pH 7) containing 1 g L^{-1} BSA to estimate the electrochemical properties of the DLC electrodes in physiological fluids containing proteins (Fig. 3). At the GC electrode, the anodic peak potential of AA in BSA-containing PBS shifted toward a more positive potential by 0.2 V from that in BSA-free PBS. In addition, as the immersion time in the BSA-containing PBS increased from 30 min to 3 h, the peak potential at the GC electrode continued to shift in a

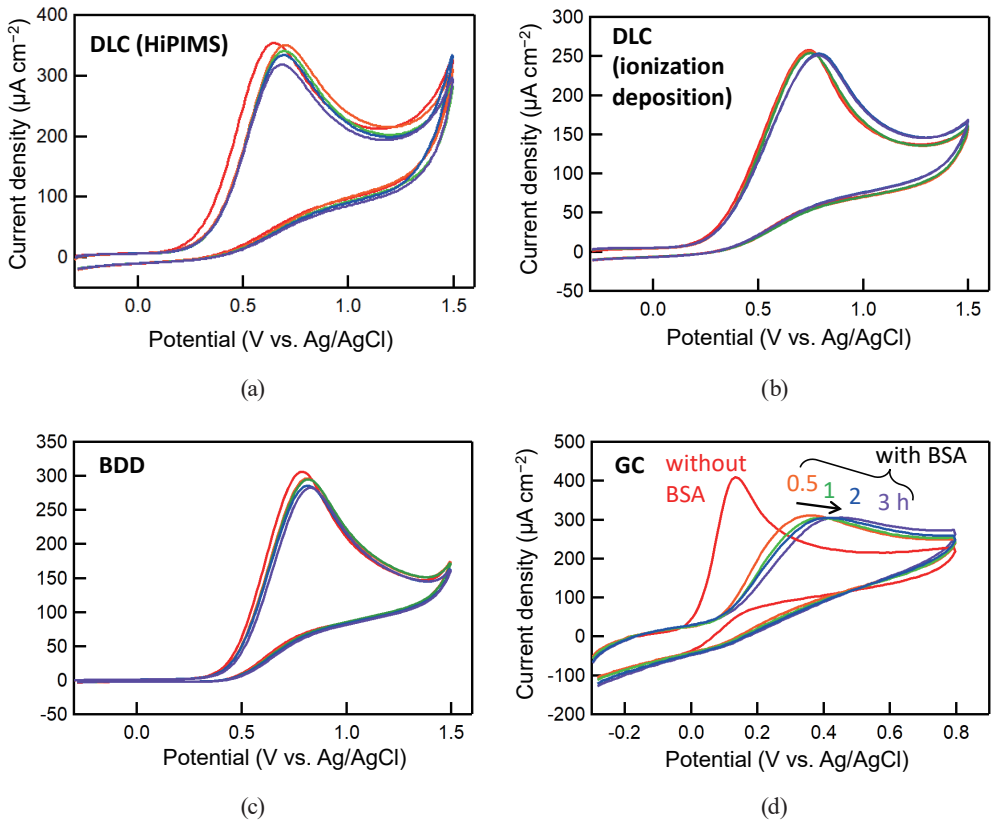

Fig. 3. (Color online) CVs of 1 mM AA in 1/15 M PBS with or without 1 g L^{-1} BSA at (a) DLC (HiPIMS), (b) DLC (ionization deposition), (c) BDD, and (d) GC electrodes. For the electrolyte containing BSA, CVs were recorded at 30 min, 1 h, 2 h, and 3 h after electrode immersion in the electrolyte. The potential sweep rate was 100 mV s^{-1}.

positive direction, accompanied by a reduction in peak current density. This phenomenon can be attributed to electrode fouling caused by the adsorption of BSA onto the GC electrode surface. In contrast, the BDD and DLC electrodes displayed remarkable stability in terms of the peak potential and peak current density of AA oxidation, regardless of the presence or absence of BSA in the electrolyte and the immersion time of the electrodes in the BSA-containing electrolyte. These findings align with those of a previous study by Shin *et al.*, who reported that square-wave voltammograms of AA at BDD electrodes exhibited resistance to fouling even in electrolytes containing BSA, gelatin, and Triton X-100.[24] This suggests that unlike electrode materials primarily composed of sp^2 carbon, such as GC electrodes and carbon paste electrodes, the DLC electrode, despite containing sp^2 carbon, maintains a surface resistant to fouling, especially by soluble substances such as proteins, similar to the BDD electrode.

To investigate the effect of DLC electrode surface modification on its resistance to BSA fouling, we treated the DLC electrode surface with UV/ozone oxidation. Figure 4 shows XPS wide spectra of an as-prepared DLC thin film and a DLC thin film treated with UV/ozone for 30 min. Both spectra showed intense C 1*s* and O 1*s* peaks. However, after UV/ozone treatment, the intensity of the O 1*s* peak relative to the C 1*s* peak increased, leading to an elevated O/(O + C) atomic concentration ratio, which increased from 0.10 for the as-prepared DLC to 0.22 for the UV/ozone-treated DLC, suggesting an increase in the amount of oxygen-containing surface functional groups in DLC electrodes owing to the treatment. Further corroborating these findings, water contact angle measurements revealed that the as-prepared DLC surface was hydrophobic with a contact angle of 81.4°. In contrast, after the UV/ozone treatment, the DLC surface changed to an improved hydrophilic state with a contact angle of 26.0°. These results collectively indicate that oxidation of the DLC surface through UV/ozone treatment increased the amount of oxygen-containing functional groups on the surface, resulting in a hydrophilic surface.

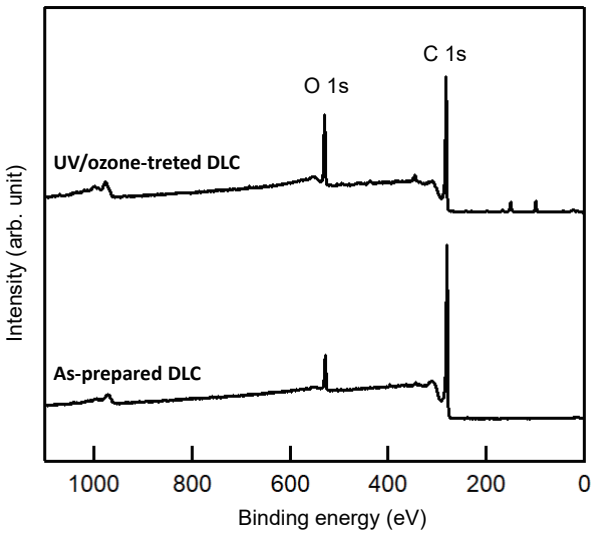

Fig. 4. XPS spectra of as-prepared and UV/ozone-treated DLC thin films (HiPIMS).

We conducted a comparative analysis of the CV of AA in PBS with or without BSA at both as-prepared DLC and UV/ozone-treated DLC electrodes [Fig. 5(a)]. There were no substantial differences in the oxidation peak potential and peak current density between the presence and absence of BSA for both electrodes. However, a notable stability enhancement was observed for the UV/ozone-treated DLC electrode, indicated by a smaller shift of the anodic peak potential of AA than for the as-prepared DLC electrode [Fig. 5(b)]. Protein fouling on electrode surfaces is often affected by hydrophobic and electrostatic interactions between proteins and the electrode surface.[25] The water contact angle measurements revealed that the UV/ozone treatment considerably improved the hydrophilicity of the DLC electrode surface, making it less susceptible to protein adsorption through hydrophobic interactions than the as-prepared surface. In addition, the XPS results suggested that the UV/ozone treatment generated oxygen-containing functional groups (C–OH, C=O, etc.) on the DLC electrode surface. These functional groups are considered to generate a surface dipole, which is negatively polarized from the electrode to the electrolyte side. Consequently, this generates electrostatic repulsion between the electrode surface and BSA, which is negatively charged in a neutral aqueous solution. This electrostatic repulsion effect further contributes to suppressing BSA adsorption on the DLC surface. Although as-deposited DLC exhibited some resistance to BSA adsorption, the surface treatment offers the potential for further enhancement of this property. The slight positive shift of the anodic peak potential (E_{pa}) of AA is considered to be also based on the electrostatic repulsion between AA and UV/ozone-treated DLC surface.[26]

3.2 Conductive DLC-MN electrode

Conductive DLC has emerged as a promising electrode material for electrochemical measurements in electrolytes containing proteins. Therefore, we developed a DLC-MN electrode for local electrochemical measurement using a DLC electrode. Figure 6 shows the SEM image of

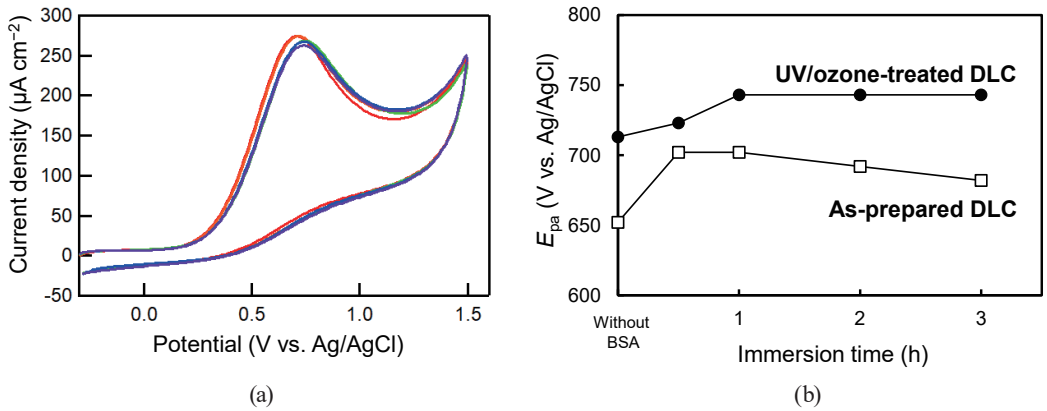

Fig. 5. (Color online) (a) CVs of 1 mM AA in 1/15 M PBS with or without 1 g L^{-1} BSA at UV/ozone-treated DLC (HiPIMS) thin-film electrode. For the electrolyte containing BSA, CVs were recorded at 30 min, 1 h, 2 h, and 3 h after electrode immersion in the electrolyte. The potential sweep rate was 100 mV s^{-1}. (b) Anodic peak potential of AA (E_{pa}) as a function of immersion time in the BSA-containing electrolyte. Data were created from Figs. 3(a) and 5(a).

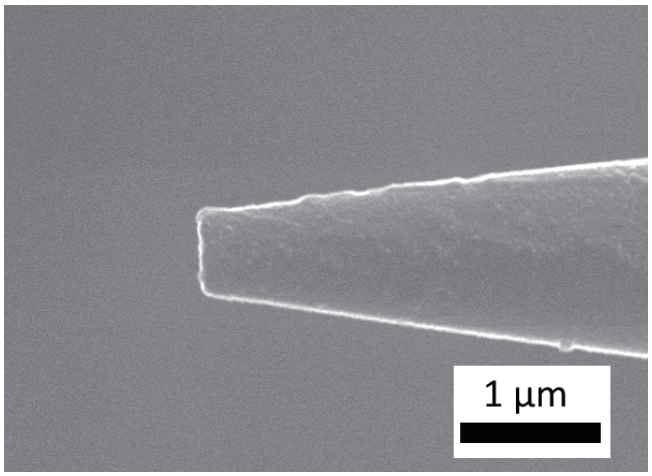

Fig. 6. SEM image of DLC-MN electrode tip.

the tip of the DLC-MN electrode. Although the tip appears flattened, possibly indicating that the tip of the glass needle substrate was broken during the DLC deposition process (before DLC deposition), the tip diameter still remained small at 600 nm. This achievement can be attributed to the exceptional characteristics of DLC as an amorphous material with low surface roughness, allowing for the deposition of a thin film with a thickness of ~75 nm while maintaining its excellent uniformity. In contrast, the crystalline nature of BDD and the inferior flatness of the BDD film compared with DLC pose challenges in forming such a thin, uniform BDD film, limiting its ability to yield electrodes with this specific shape. In addition, BDD thin-film deposition requires a chemical vapor deposition process at 800 °C or higher temperatures, rendering it unsuitable for film formation on glass needles. Therefore, the ability to fabricate such microneedle electrodes is an advantage of DLC over BDD. For example, the typical size of a cell is ~20 μm; thus, the application of such microneedle electrodes is expected to enable local electrochemical measurements in the vicinity of a single cell.

Figure 7(a) shows the CV of AA in PBS at the DLC-MN electrode, displaying a sigmoidal shape characteristic of microelectrodes. The length of the DLC-MN electrode in contact with the electrolyte was 1 cm. Therefore, the CV current is considered to be controlled through cylindrical diffusion. Furthermore, as the AA concentration changed, the limiting current exhibited a linear increase, affirming a proportional response to changes in AA concentration. Figure 7(b) shows the CV of AA in PBS containing 1 g L^{-1} BSA at the DLC-MN electrode, where the sigmoidal CV response remained consistent with that in the case without BSA, and the limiting current value (at +1.3 V vs Ag/AgCl) displayed a negligible decrease of, at most, 8%. This observation underscores the effective suppression of electrode fouling by BSA at the DLC-MN electrode, mirroring the results of the planar electrode examinations. Moreover, the calibration curve representing a constant current against the AA concentration shows good linearity, affirming the potential of the DLC-MN electrode for quantitative electrochemical analysis. Microelectrodes enable local electrochemical measurements and offer enhanced

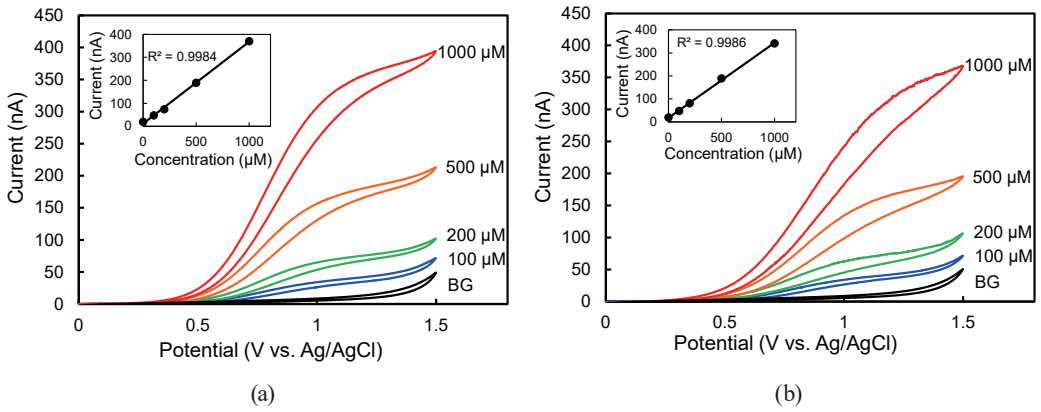

Fig. 7. (Color online) CV of 1/15 M PBS containing various concentrations of AA (a) without and (b) with 1 g L^{-1} BSA at DLC-MN electrode. The potential sweep rate was 10 mV s^{-1}. The inset displays the calibration curve showing the anodic current at 1.3 V vs Ag/AgCl as a function of AA concentration.

sensitivity by increasing the signal-to-background ratio compared with CV currents obtained from planar electrodes based on linear diffusion. Furthermore, the utilization of DLC as the electrode material holds the promise of mitigating protein fouling. Therefore, the DLC-MN electrode is suitable for achieving high-sensitivity local electrochemical detection in complex biological fluids.

Next, the CV of theophylline (TP) was performed at the DLC-MN electrode. TP, known as an antiasthma drug, operates within a narrow therapeutic range in the bloodstream. Therefore, to administer effective medication, monitoring the TP concentration in the blood is necessary through constant blood collection, precise medication administration timing, and maintaining the blood TP concentration within the therapeutic range (therapeutic drug monitoring, TDM). Therefore, the ability to electrochemically measure blood TP concentration could revolutionize TDM, providing a rapid and precise approach. TP is known to be detected electrochemically based on the two-electron oxidation.[27] Figure 8 shows the CV of TP in PBS with and without 1 g L^{-1} BSA at the DLC-MN electrode. It was confirmed that the anodic current of TP rose from approximately +1.2 V vs. Ag/AgCl and exhibited an anodic current increment proportional to the TP concentration for both cases. The anodic current at +1.45 V vs Ag/AgCl was plotted against the TP concentration, revealing excellent linearity in the range of 100–500 μM for both cases. Although the presence of BSA in PBS slightly decreased the anodic current (within a 15% range) compared with PBS without BSA, the linear response of the anodic current remained intact. This indicates that the DLC-MN electrode can accurately quantify TP concentration even in protein-containing electrolyte solutions. Therefore, the DLC-MN electrode emerges as a useful electrode material to realize an electrochemical TDM system for TP.

Finally, we compared the AA detection properties of the DLC-MN electrode and platinum microelectrode (Pt-ME) by constant-potential electrolysis in PBS with and without BSA. Figure 9 shows the constant-current electrolysis current when introducing 200 μL of 10 mM AA to 1/15 M PBS. The observed current fluctuation originated from stirring the electrolyte during the measurement. In PBS without BSA, the addition of AA solution to the electrolyte led to a

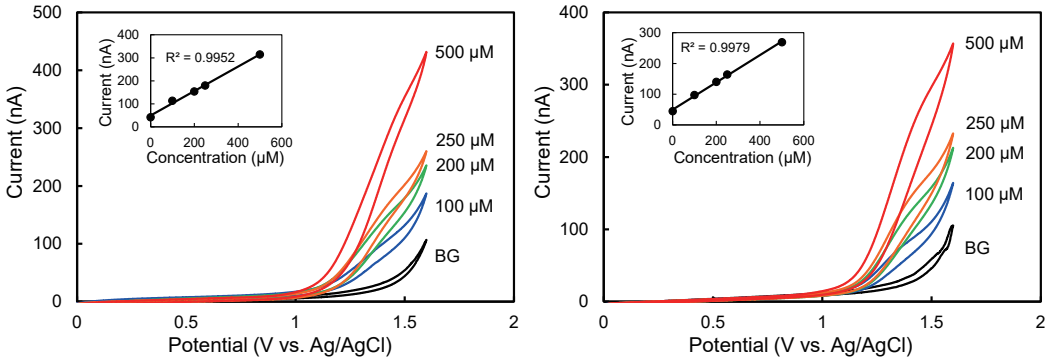

(a) (b)

Fig. 8. (Color online) CV of TP in 1/15 M PBS (a) without and (b) with 1 g L^{-1} BSA at DLC-MN electrode. The TP concentrations tested were 0, 100, 200, 250, and 500 μM. The potential sweep rate was 10 mV s^{-1}. The inset displays the calibration curve showing the anodic current at 1.45 V vs. Ag/AgCl as a function of TP concentration.

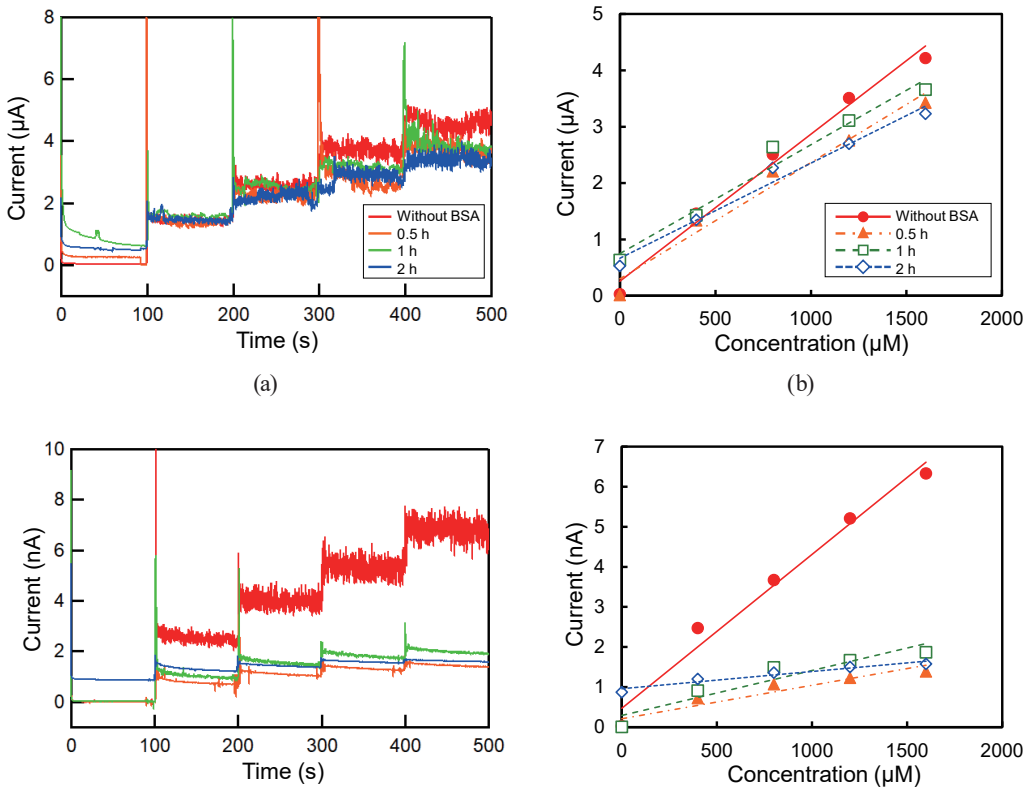

(a) (b) (c) (d)

Fig. 9. (Color online) Current response to AA injection into 1/15 PBS with or without 1 g L^{-1} BSA in constant-potential electrolysis at (a) DLC-MN and (c) Pt-ME. The constant potential was set at 1.2 and 0.8 V vs Ag/AgCl for DLC-MN and Pt-ME, respectively. For the electrolyte containing BSA, the current was recorded at 30 min, 1 h, and 2 h after immersion of the electrode in the electrolyte. Calibration curves showing current response as a function of AA concentration at (b) DLC-MN and (d) Pt-ME.

stepwise increase in the steady-state anodic current, with the current rising in direct proportion to the AA concentration in the electrolyte [Fig. 9(a)]. A similar pattern emerged in PBS containing 1 g L^{-1} BSA, where a linear increase in steady-state anodic current correlated with increasing AA concentration, mirroring the behavior of the system without BSA. However, the slope of the calibration curve decreased with the immersion time of the electrode in the BSA-containing electrolyte, reaching 65% of the slope observed without BSA after 2 h of immersion of the electrode in the BSA-containing electrolyte [Fig. 9(b)]. Although a decrease in the slope of the calibration curve was observed, the rate of decrease slowed with respect to the immersion time. In contrast, when the same experiment was conducted with Pt-ME, a noticeable difference was observed between PBS with and without BSA [Fig. 9(c)]. Without BSA, Pt-ME demonstrated a good linearity of the anodic current with AA concentration. However, in the presence of BSA, a notable decrease in current occurred after a 30 min immersion of the electrode in BSA-containing electrolyte (<30% of the system without BSA). In addition, the linearity of the anodic current with respect to AA concentration deteriorated [Fig. 9(d)]. This deterioration in current response can be attributed to nonspecific protein adsorption, a common issue on metal surfaces such as platinum, causing electrode fouling.[25] In direct comparison, the DLC-MN electrode has superior stability in its anodic current. These results suggest that the DLC-MN electrode can be applied to electrochemical detection in protein-containing electrolytes through constant-potential electrolysis with a stable current.

4. Conclusions

The electrochemical properties of DLC thin-film electrodes fabricated using HiPIMS and ionization deposition methods were investigated. Comparative analysis of the CV at the BDD thin-film, GC, and DLC electrodes revealed that the DLC electrodes exhibited electrochemical properties similar to those of BDD electrodes, showing a wide potential window and relatively low background current. Notably, in PBS containing BSA, the DLC electrode displayed minimal signs of electrode fouling, distinguishing them from the GC electrodes. DLC can form thin, uniform, flat films on various substrate materials through a low-temperature process. Taking advantage of these properties, we created DLC-MN by coating the tip of a glass needle substrate with conductive DLC. Similar to their planar DLC thin-film counterparts, the DLC-MN electrodes hold promise for the electrochemical sensing of electroactive substances in biological fluids because they are resistant to electrode fouling, even in PBS containing BSA. In particular, the possibility of fabricating MN electrodes with a tip diameter as small as 600 nm paves the way for their potential application in highly sensitive electrochemical devices. These devices have the potential for minimally invasive electrochemical sensing and monitoring, as well as electrochemical measurements in or in the vicinity of a single cell.

References

1 F. Tasca, C. Tortolini, P. Bollella, and R. Antiochia: Curr. Opin. Electrochem. **16** (2019) 42. https://doi.org/10.1016/j.coelec.2019.04.003
2 P. Dardano, I. Rea, and L. De Stefano: Curr. Opin. Electrochem. **17** (2019) 121. https://doi.org/10.1016/j.coelec.2019.05.012
3 J. Madden, C. O'Mahony, M. Thompson, A. O'Riordan, and P. Galvin: Ses. Bio-Sens. Res. **29** (2020) 100348. https://doi.org/10.1016/j.sbsr.2020.100348
4 S. Sharma, Z. Huang, M. Rogers, M. Boutelle, and A. E. G. Cass: Anal. Bioanal. Chem. **408** (2016) 8427. https://doi.org/10.1007/s00216-016-9961-6
5 S. R. Chinnadayyala, J. park, A. T. Satti, D. Kim, and S. Cho: Electrochim. Acta **369** (2021) 137691. https://doi.org/10.1016/j.electacta.2020.137691
6 H. Teymourian, C. Moonla, F. Tehrani, E. Vargas, R. Aghavali, A. Barfidokht, T. Tangkuaram, P. P. Mercier, E. Dassau, and J. Wang: Anal. Chem. **92** (2020) 2291. https://doi.org/10.1021/acs.analchem.9b05109
7 A. M. V. Mohan, J. R. Windmiller, R. K. Mishra, and J. Wang: Bosens. Bioelectron. **91** (2017) 574. https://doi.org/10.1016/j.bios.2017.01.016
8 K. Y. Goud, C. Moonla, R. K. Mishra, C. Yu, R. Narayan, I. Litvan, and J. Wang: ACS Sens. **4** (2019) 2196. https://doi.org/10.1021/acssensors.9b01127
9 J.-X. Zhou, L.-N. Tang, F. Yang, F.-X. Liang, H. Wang, Y.-T. Li, and G.-J. Zhang: Analyst **142** (2017) 4322. https://doi.org/10.1039/C7AN01446E
10 N. V. Apollo, M. I. Maturana, W. Tong, D. A. X. Nayagam, M. N. Shivdasani, J. Foroughi, G. G. Wallace, S. Prawer, M. R. Ibbotson, and D. J. Garrett: Adv. Fnct. Mater. **25** (2015) 3551. https://doi.org/10.1002/adfm.201500110
11 J. R. Windmiller, N. Zhou, M.-C. Chuang, G. Valdés-Ramírez, P. Santhosh, P. R. Miller, R. Narayan, and J. Wang: Analyst **136** (2011) 1846. https://doi.org/10.1039/C1AN00012H
12 A. Suzuki, T. A. Ivandini, K. Yoshimi, A. Fujishima, G. Oyama, T. Nakazato, N. Hattori, S. Kitazawa, and Y. Einaga: Anal. Chem. **79** (2007) 8608. https://doi.org/10.1021/ac071519h
13 K. Asai, T. A. Ivandini, and Y. Einaga: Sci. Rep. **6** (2016) 32429. https://doi.org/10.1038/srep32429
14 G. Ogata, Y. Ishii, K. Asai, Y. Sano, F. Nin, T. Yoshida, T. Higuchi, S. Sawamura, T. Ota, K. Hori, K. Maeda, S. Komune, K. Doi, M. Takai, I. Findlay, H. Kusuhara, Y. Einaga, and H. Hibino: Natur. Biomed. Eng. **1** (2017) 654. https://doi.org/10.1038/s41551-017-0118-5
15 Y. Ohgoe, K. K. Hirakuri, H. Saitoh, T. Nakahigashi, N. Ohtake, A. Hirata, K. Kanda, M. Hiratsuka, and Y. Fukui: Surf. Coat. Technol. **207** (2012) 350. https://doi.org/10.1016/j.surfcoat.2012.07.018
16 Y. Tanaka, M. Furuta, K. Kuriyama, R. Kuwabara, Y. Katsuki, T. Kondo, A. Fujishima, and K. Honda: Electrochim. Acta **56** (2011) 1172. https://doi.org/10.1016/j.electacta.2010.11.006
17 A. Zeng, V. F. Neto, J. J. Gracio and Q. H. Fan: Diam. Relat. Mater. **43** (2014) 12. https://doi.org/10.1016/j.diamond.2014.01.003
18 C.-W. Liu, W.-E. Chen, Y. T. A. Sun, and C.-R. Lin: Appl. Surf. Sci. **436** (2018) 967. https://doi.org/10.1016/j.apsusc.2017.12.035
19 A. Liu, Q. Ren, T. Xu, M. Yuan, and W. Tang: Sens. Actuators, B **162** (2012) 135. https://doi.org/10.1016/j.snb.2011.12.050
20 M. Hiratsuka, A. Azuma, H. Nakamori, Y. Kogo, and K. Yukimura: Surf. Coat. Technol. **229** (2013) 46. https://doi.org/10.1016/j.surfcoat.2012.06.016
21 T. Kondo, S. Aoshima, K. Honda, Y. Einaga, A. Fujishima, and T. Kawai: J. Phys. Chem. C **111** (2007) 12650. https://doi.org/10.1021/jp0727704
22 S. Miyagawa, S. Nakao, J. Choi, M. Ikeyama, and Y. Miyagawa: New Diam. Front. Carbon Technol. **16** (2006) 33.
23 T. Kondo, H. Ito, K. Kusakabe, K. Ohkawa, K. Honda, Y. Einaga, A. Fujishima, and T. Kawai: Diam. Relat. Mater. **17** (2008) 48. https://doi.org/10.1016/j.diamond.2007.10.009
24 D. Shin, D. A. Tryk, A. Fujishima, A. Merkoçi, and J. Wang: Electroanalysis **17** (2005) 305. https://doi.org/10.1002/elan.200403104
25 B. L. Hanssen, S. Siraj, and D. K. Y. Wong: Rev. Anal. Chem. **35** (2016) 1. https://doi.org/10.1515/revac-2015-0008
26 E. Popa, Y. Kubota, D. A. Tryk, and A. Fujishima: Anal. Chem. **72** (2000) 1724. https://doi.org/10.1021/ac990862m
27 R. D. Crapnell and C. E. Banks: Talanta Open **3** (2021) 100037. https://doi.org/10.1016/j.talo.2021.100037